inter.noise
HAMBURG 2016

Enhanced Acoustic Black Hole Effect Using a Modified Thickness Profile

Liling TANG[1]; Li CHENG[1*]; Hongli JI[2]; Jinhao QIU[2]

[1] Department of Mechanical Engineering, The Hong Kong Polytechnic University, Hong Kong,

[2] State Key Laboratory of Mechanics and Control of Mechanical Structures, Nanjing University of Aeronautics and Astronautics, China

ABSTRACT

The phenomenon of Acoustics Black Hole (ABH) takes place when bending waves propagate inside a think-walled structure with a power-law thickness profile. The phenomenon as well as its application potential in vibration damping enhancement, noise control and energy harvesting has also been demonstrated theoretically and experimentally by recent research. However, manufacturing an ideally tailored power-law profile can hardly be achieved in practice. The unavoidable truncation at the wedge tips of the structure can significantly weaken the ABH effect. On the premise of the minimum achievable truncation thickness by current manufacturing technology, ways to ensure and achieve better ABH effect need to be explored. In this paper, we investigate this issue using a previously developed wavelet-decomposed semi-analytical model on an Euler-Bernoulli beam with a modified power-law profile. As a continuation of the previous work, the model was first validated experimentally using a truncated conventional ABH profile. Then, the modified thickness profile is numerically investigated in terms of system loss factor and energy distribution. Compared with the conventional thickness profile with the same truncated wedge tip, it is shown that the modified thickness profile, along with the use of an extended plateau at the wedge tip, brings about a systematic increase in the ABH effect at mid-to-high frequencies, whilst providing rooms for possible low frequency applications.

Keywords: Acoustic Black Hole, modified thickness profile, damping enhancement.

1. INTRODUCTION

The Acoustics Black Holes (ABH) effect utilizes the bending wave propagation properties inside a thin-walled structure with a tailored power-law thickness variation, where the phase velocity of the bending wave gradually reduces to zero, resulting in zero wave reflection in the ideal scenario [1, 2]. Owing to the high energy concentration within a confined area in the structure, its appealing potential in applications such as passive vibration control [3-8], sound radiation control [9, 10] and energy harvesting [11, 12] arouses the interest of researchers. In the realization, however, ideal thickness profile with extreme thin thickness at the wedge tip can hardly manufactured. This leads to the unavoidable truncation, which, albeit very small, would significantly compromise the ideal ABH effect by increasing wave reflections [2]. To maximize the ABH effect with the conventional thickness profile, the truncated tip needs to be as small as possible, which results in high manufacturing cost and would also lead to tip damage of tearing and irregularities. Although a few researches showed that the damage on the wedge tip may not be a serious problem in terms of the ABH effect [13-14]; structures with ultra-thin or damaged tips however can hardly be applied in industry due to the structural strength problems. Therefore, on the premise of the minimum achievable truncation thickness by currently available manufacturing technology, ways to ensure and achieve better ABH effect need to be explored.

Motivated by this, a modified thin wedge with extended constant thickness is proposed and analyzed by experiment and FEM analyses [15]. Meanwhile, various modified wedge thickness profiles were also proposed [12, 16]. Probably due to the lack of flexible model, systematic analyses

* li.cheng@polyu.edu.hk

on the topic have not been conducted.

In this paper, ways to achieve better ABH effect on the premise of the minimum achievable truncation thickness and the possibility of applying ABH effect at low frequencies are investigated. A Euler-Bernoulli beam with a modified thickness profile and an extended platform is studied using a previously developed wavelet-decomposed model [17]. After experimental validation, the model is used to investigate effect of some key parameters defining the modified thickness profile. Effect of an extended platform is also discussed in views of possible extension of the ABH effect to the low frequency.

2. THEORETICAL MODEL AND ITS EXPERIMENTAL VALIDATION

An Euler-Bernoulli beam with a symmetrical thickness profile is considered (Fig. 1). The beam consists of a uniform part with a constant thickness h_b from x_{b3} to x_{b4}, and an ABH portion with a modified thickness profile, $h(x)=\varepsilon(x-x_0)^m+h_0$, from x_{b2} to x_{b3}. This modified thickness profile will retreat to the conventional power -law thickness profile, *i.e.* $h(x)=\varepsilon x^m$, when x_0 and h_0 are both set to zero. A platform of uniform thickness $h(x_{b2})$ is extended from the truncation point x_{b2} to point x_{b1}. The beam is covered by two damping layers with variable thickness $h_d(x)$ from x_{d1} and x_{d2}. A point force $f(t)$ is applied at x_f and response is evaluated at x_m. The beam is free at the right-hand-side end and elastically supported by artificial translational and rotational springs [18, 19] at the other, the stiffness of which can be adjusted to achieve various boundary conditions. The damping of both the beam and the damping layer are taken into account through complex stiffness E, *i.e.*, $E=E(1+i\eta)$, where η is the damping loss factor of the respective materials. A previously developed wavelet-decomposed model based on Lagrange's equation is used to obtain the vibration response [17]. The modelling principle is briefly recalled in the following.

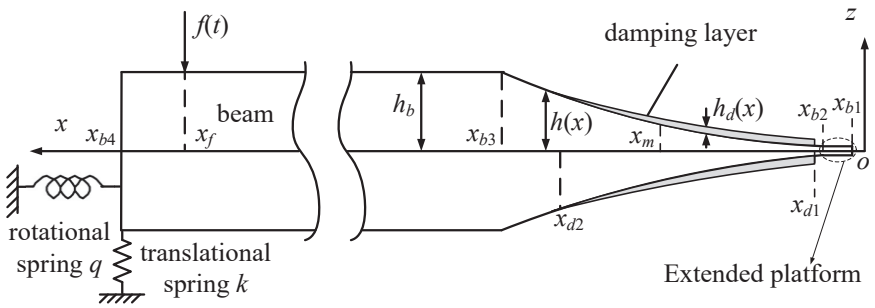

Fig. 1 An Euler-Bernoulli beam with symmetrical modified power-law profile and extended platform.

Based on the Euler-Bernoulli beam theory, the displacement field of the beam is expressed as

$$\{u,w\}=\left\{-z\frac{\partial w}{\partial x},w(x,t)\right\} \tag{1}$$

where the vector $\{u,w\}$ denotes the displacement of a point either on the beam or on the damping layers under the assumption of perfect bonding between them. w can be decomposed over the basis of the Mexican hat wavelets (MHW) [20] $\varphi_{j,k}(x)$ as

$$w(x,t)=\sum_{j=0}^{m}\sum_{k}a_{j,k}(t)\varphi_{j,k}(x) \tag{2}$$

where $\varphi_{j,k}(x)=\frac{2}{\sqrt{3}}\pi^{-\frac{1}{4}}2^{j/2}[1-(2^j x-k)^2]\mathrm{e}^{-\frac{(2^j x-k)^2}{2}}$; j is the scaling parameter (integer) to stretch or squeeze the MHW and k the translation parameter (integer) to move the MHW along x axis.

The Lagrangian of the system L writes

$$L=E_k-E_p+W \tag{3}$$

where E_k presents the kinetic energy of the system; E_p the potential energy and W the work done by the excited force, expressed as

$$E_k = \frac{1}{2}\int \rho \left(\frac{\partial w}{\partial t}\right)^2 \mathrm{d}V \tag{4}$$

$$E_p = \frac{1}{2}\int EI(x)\left(\frac{\partial^2 w}{\partial x^2}\right)^2 \mathrm{d}x + \frac{1}{2}kw(x_{b4},t)^2 + \frac{1}{2}q\left(\frac{\partial w(x_{b4},t)}{\partial x}\right)^2 \tag{5}$$

$$W = f(t)\cdot w(x_f,t) \tag{6}$$

The extremalization of Hamiltonian function leads to the following Lagrange's equations

$$\frac{\mathrm{d}}{\mathrm{d}t}\left(\frac{\partial L}{\partial \dot{a}_{j,k}(t)}\right) - \frac{\partial L}{\partial a_{j,k}(t)} = 0 \tag{7}$$

Substituting Eqs. (3) to (6) into Eq. (7) yields the following linear equations

$$\mathbf{M}\ddot{\mathbf{a}}(t) + \mathbf{K}\mathbf{a}(t) = \mathbf{f}(t) \tag{8}$$

where **M** and **K** are, respectively, the mass matrix and stiffness matrix; **a**(t) and **f**(t) are, respectively, the vectors of the response $a_{ij}(t)$ and the force, which can be expressed as $\mathbf{a}(t) = \mathbf{A}e^{j\omega t}$ and $\mathbf{f}(t) = \mathbf{F}e^{j\omega t}$ in harmonic regime. Then Eq. (8) can be rewritten as

$$[\mathbf{K} - \omega^2\mathbf{M}]\mathbf{A} = \mathbf{F} \tag{9}$$

Solving Eq. (9) yields the forced vibration response. Setting the force vector in Eq. (9) to zero, we can obtain the natural frequencies and the corresponding mode shapes from the following eigenvalue equation

$$\mathbf{M}^{-1}\mathbf{K}\mathbf{A} = \omega^2\mathbf{A} \tag{10}$$

where the eigenvalues take complex forms as $\omega^2 = \omega_n^2(1+i\eta)$ with η being the corresponding modal loss factor of the system.

The model is first validated experimentally using a free-free beam with conventional ABH thickness profile without the extended platform, as illustrated in Fig. 2. The parameters of the ABH part are: ε =0.00125 and m=2 with tip thickness $h(x_{b2})$=0.02 cm. The uniform part has a thickness h_b=0.32 cm and is 16 cm long. The whole beam has a uniform width of 1 cm and is made of steel with a mass density of 7794 kg/m^3 and Young modulus of 200 Gpa. The beam was suspended by two thin strings to mimic the free boundary conditions. A point force, with a periodic chirp signal from 0 Hz to 12 kHz was generated by an electromagnetic shaker at x_f=26 cm, and measured through a force transducer (B&K 8200). A Polytec scanning laser vibrometer (PSV) was used to measure the beam response at two representative points located in ABH part and uniform part, x_m=5 cm and 20 cm, respectively.

Fig. 3 compares the calculated cross point mobility ($\dot{w}(x_m)/f(x_f)$) with the experimental results. As can be seen, the simulation results agree very well with experimental ones, both in amplitude and peak locations, especially for the frequency range below 9000 Hz with an error typically less than 2% in terms of natural frequencies. The increasing error in higher frequencies is likely due to the neglected shear and torsional effect in the model, which certainly exists at higher frequencies and may be aggravated by the deviation of the excited force from the enteral axis. In general, the proposed model guarantees high accuracy as compared with experimental results.

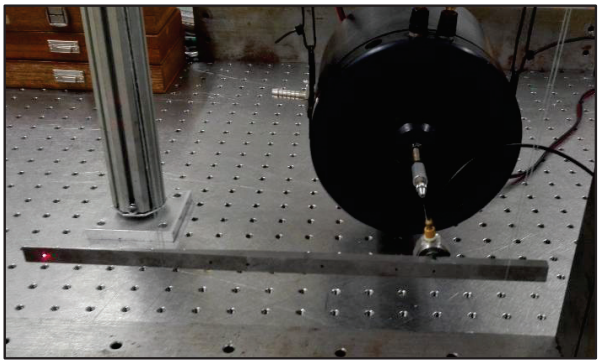

Fig. 2 Experimental set-up.

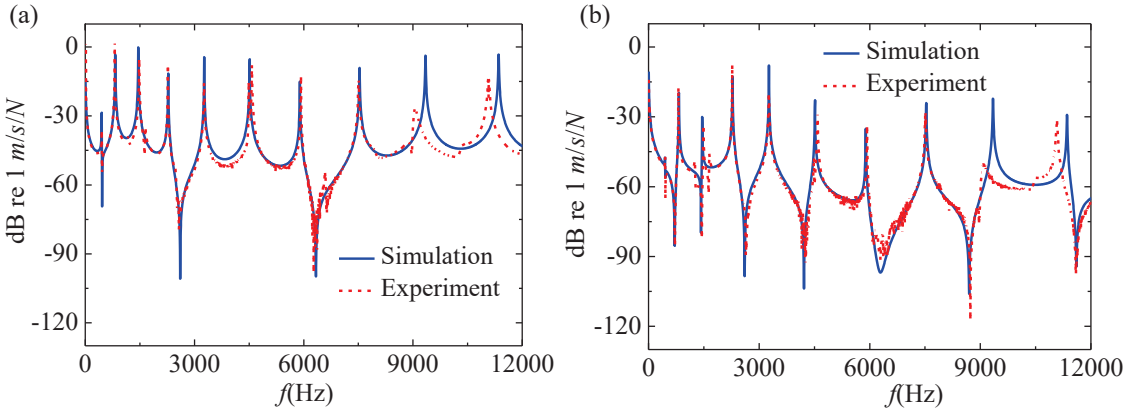

Fig. 3 Comparison of the experimental cross point mobility: (a) $\dot{w}(x_m$=5cm$) / f(x_f)$, (b) $\dot{w}(x_m$=20cm$) / f(x_f)$ against simulation results.

3. NUMERICAL SIMULATION AND DISCUSSIONS

Consider two clamped-free beams with the same uniform portion under a unit harmonic driving force applied at the point x_f, 3 cm away from the clamped end (as shown in Fig.1). The point response is calculated at the point x_m, 8 cm away from the clamped end. Keep the same truncation thickness $h(x_{b2})$ and profile parameters ε and m, the responses of the two beams are first analyzed and compared. Case 1 involves a conventional ABH thickness profile ($h_1(x) = \varepsilon x^m$) and case 2 a modified thickness profile ($h_2(x) = \varepsilon(x - x_0)^m + h_0$). The material and geometrical parameters are tabulated in Table 1. Note that truncated at x_{b2}=4 cm, the prescribed truncation thickness $h(x_{b2})$, 0.02cm, is the same in both cases. As a benchmark system, an entirely uniform beam with the same thickness and same length as case 1 is also used in the following analyses.

Table 1 - Material and geometrical parameters.

Material parameters	Geometrical parameters
Beam	
E_b = 210 GPa	ε = 0.00125 cm^{-1}
ρ_b = 7800 kg/m^3	m = 2
η_b = 0.001	x_0 = 4
Damping layers	h_0 = 0.02 cm
E_d = 5 GPa	h_b =0.32 cm
ρ_d = 950 kg/m^3	$h(x_{b2})$= 0.02 cm
η_d = 0.1	l_{Uni}= x_{b4}- x_{b3}= 12 cm

3.1 Effect of the additional thickness h_0

Keeping the inevitable tip truncation thickness $h(x_{b2})$ as the same, we first investigate the possibility of changing thickness profile to achieve better ABH effect. Compared with conventional ABH thickness profile (case 1), the modified thickness profile (case 2) possesses an additional thickness term h_0. The effect of this additional thickness term on ABH effect is first considered without the extended platform.

Fig. 4 (a) depicts the cross point mobility for three different beam cases without damping layers. It shows that the vibration level at the calculated point in beams with both the conventional and modified ABH profiles is slightly reduced at higher frequencies compared with their uniform counterpart as a result of ABH effect. The barely noticeable reduction is due to the fact that the existing truncation, as expected, generates wave reflections in the absence of the damping layers. On the other hand, a slightly higher reduction is observed at higher frequencies with the modified ABH profiles, which

indicates better ABH effect achieved by case 2. To further explain this phenomenon, the energy ratio Γ ($\Gamma = 10\log\frac{<V^2>_{\text{ABH}}}{<V^2>_{\text{Unif}}}$) between the ABH portion and the uniform portion are compared in Fig. 4 (b). Larger energy ratio means better energy concentration in the ABH part, resulting from the better ABH effect. Obviously, the higher energy ratio in case 2 at the higher frequencies confirms the slight superiority of the modified ABH profile over its conventional counterpart.

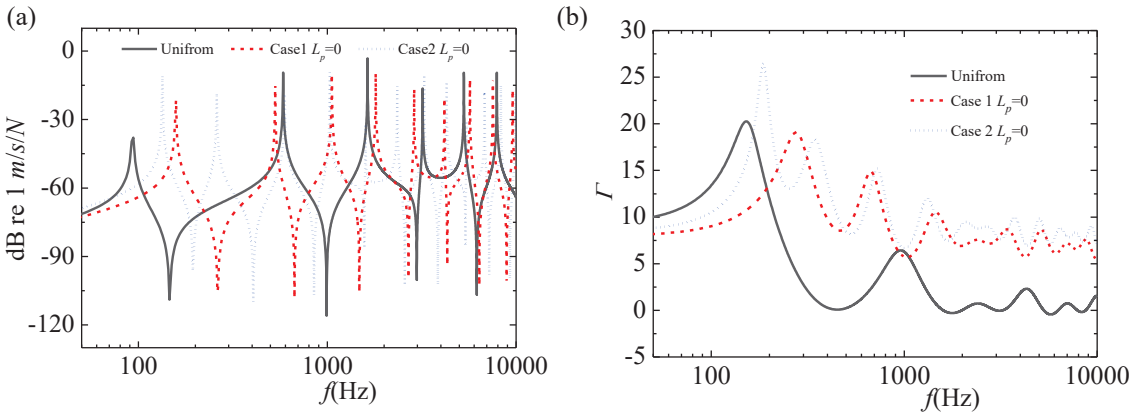

Fig. 4 (a) The cross point mobility $\dot{w}(x_m)/f(x_f)$, and (b) the ratio of the mean quadratic velocity of the ABH portion to the uniform beam portion for three different beam cases without damping layers.

When the ABH parts are covered with damping layers having the same thickness h_d=0.02 cm, the system loss factors of the above three beams are compared in Fig. 5. With comparison of the uniform beam, the system damping loss factor of case 1 is significantly increased at higher frequencies due to the ABH effect, while that of case 2 is nearly doubled. Unlike case 1 with conventional thickness profile, case 2 with the modified profile also increase the lower-order modal loss factor noticeably. Accordingly, the amplitude reduction in the vibration level of case 2 is also more significant over the whole frequency range than that of case 1, in comparison with the uniform beam as revealed in Fig. 6(a). However, Fig. 6 (b) indicates the applied damping layers do not noticeably affect the energy distribution of the three different beams, as compared with situations without damping layers illustrated in Fig. 4 (b).

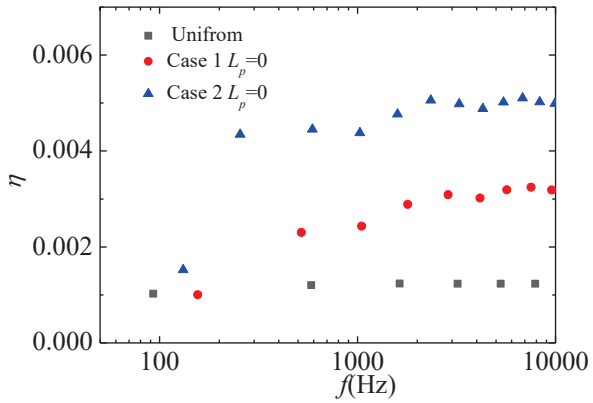

Fig. 5 Comparison of the system loss factors for three different beam cases with the ABH part covered by damping layers (h_d = 0.02 cm).

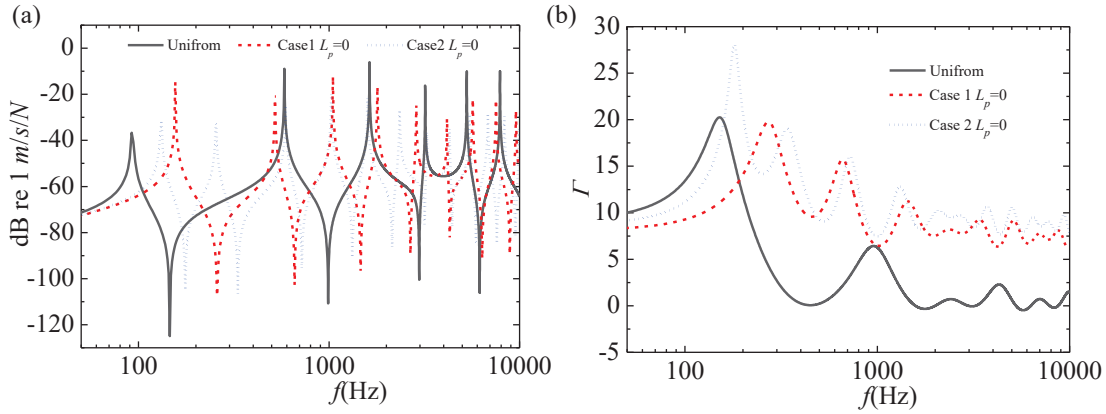

Fig. 6 (a) The cross point mobility $\dot{w}(x_m)/f(x_f)$, and (b) the ratio of the mean quadratic velocity of the ABH portion to the uniform beam portion for three different beam cases with damping layers (h_d = 0.02 cm).

A comparison of the mode shapes in Fig. 7 could explain the possible reason why the modified thickness profile with an additional thickness h_0 outperforms the conventional ABH profile for the same given thickness truncation. As can be seen, case 2 with the modified profile promotes larger structural deformation at the ABH portion for both the first and one representative higher-order (tenth) mode. Therefore, more energy would concentrate on the ABH part, which is beneficial to energy absorption by the damping layers.

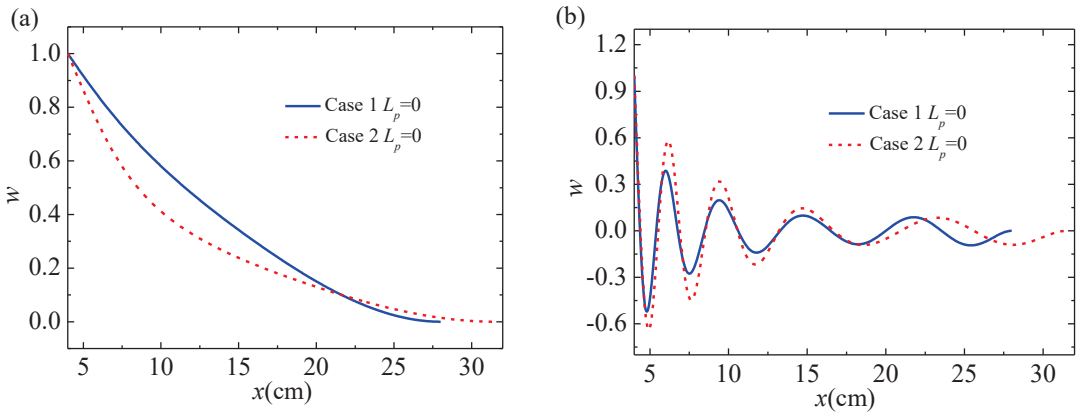

Fig. 7 (a) First mode shape, and (b) tenth mode shape comparison for two cases.

3.2 Effect of the extended platform

The truncated tip is extended to form a platform of constant thickness both in the conventional and modified thickness profiles discussed above to explore the possibility of improving ABH effect at both high and low frequencies. Fig. 8 compares the system loss factors of two cases with and without the extended platform when damping layers are applied over the ABH parts (extended platforms are also considered as a part of the ABH portion for convenience). It is clear that the extended platform, with a length L_p= 4 cm, significantly increases the system damping at higher frequencies for both thickness profiles. On the other hand, the system loss factor at the lower frequencies also significantly increases with a platform, in contrast to the cases without platform. Therefore, the extended platform allows achieving better broadband ABH effect while providing the possibility to lower its effective region. Owing to the additional benefit of the additional thickness h_0 shown above, the modified thickness profile further enhances the ABH effect compared with the conventional ABH profile, as demonstrated in Fig. 8.

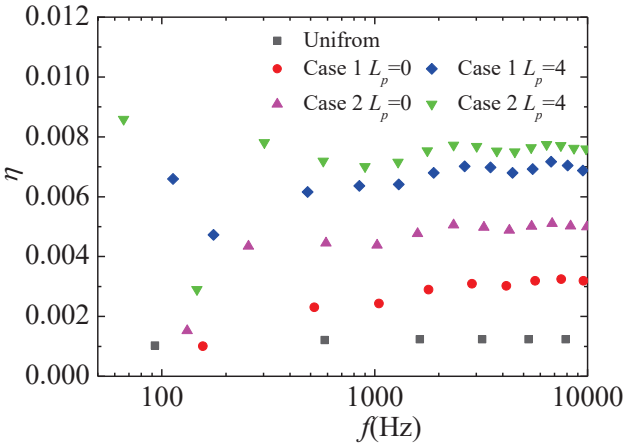

Fig. 8 Comparison of system loss factors for three different beam cases with and without extended platform when ABH part covered by damping layers (h_d = 0.02 cm).

To better assess the ABH effect achieved by the modified thickness profile, the following discussions focus on case 2. Fig. 9 depicts the cross point mobility in the uniform beam part and the energy ratio of the beams with and without platform when damping layers are applied over the tailored ABH part. From Fig. 9 (a), we can see that the amplitude of the vibration in the uniform beam part is reduced with the use of the extended platform, which is systematic at higher frequencies, but more or less at the lower resonant frequencies. The energy ratio, shown in Fig. 9 (b), is also consistent with this observation that, with the extended platform, better energy focalization in the ABH part takes place at higher frequencies, but not systematically at low frequencies. This is because the lower frequency alteration in the system damping depends more on the modal characteristics of the system. In general, however, the use of platform allows achieving better ABH effect at higher frequencies. Meanwhile, it seems to promote more effective ABH effect in the lower frequency region as well, as evidenced by the significantly increased first peak in the energy ratio curves and the corresponding much lower frequency compared with the case without platform.

The mode shape comparison with and without the extended platform in Fig. 10 also partly explains the above phenomena. The platform seems to provoke larger structural deformation at the ABH portion as compared with the case without platform at the first mode, allowing better energy concentration in the ABH portion. For higher order mode (tenth mode as an example), the extended platform prolongs the active area of the ABH by extending the intensive wave packet to the platform area after being compressed by the ABH profile.

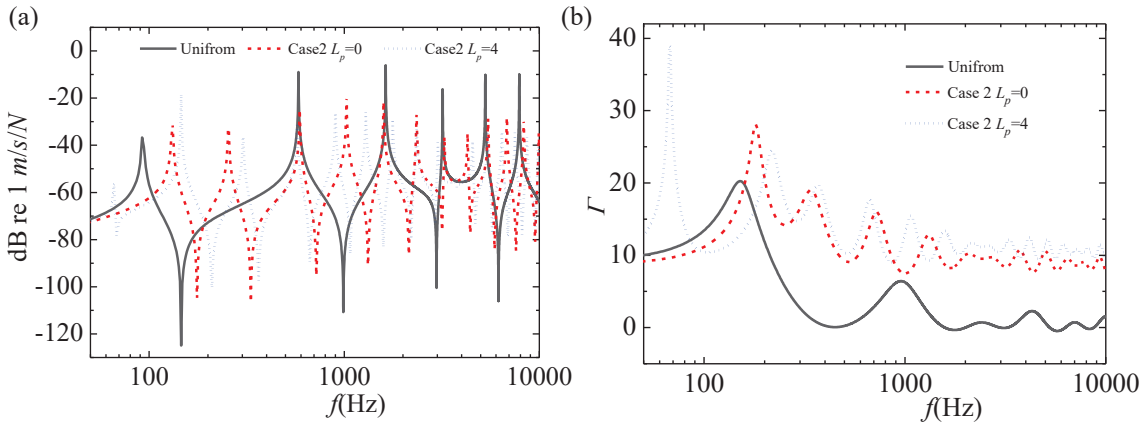

Fig. 9 The cross point mobility $\dot{w}(x_m)/f(x_f)$, and (b) the ratio of the mean quadratic velocity of the ABH portion to the uniform beam portion for case 2 with and without extended platform when ABH portion covered by damping layers (h_d = 0.02 cm).

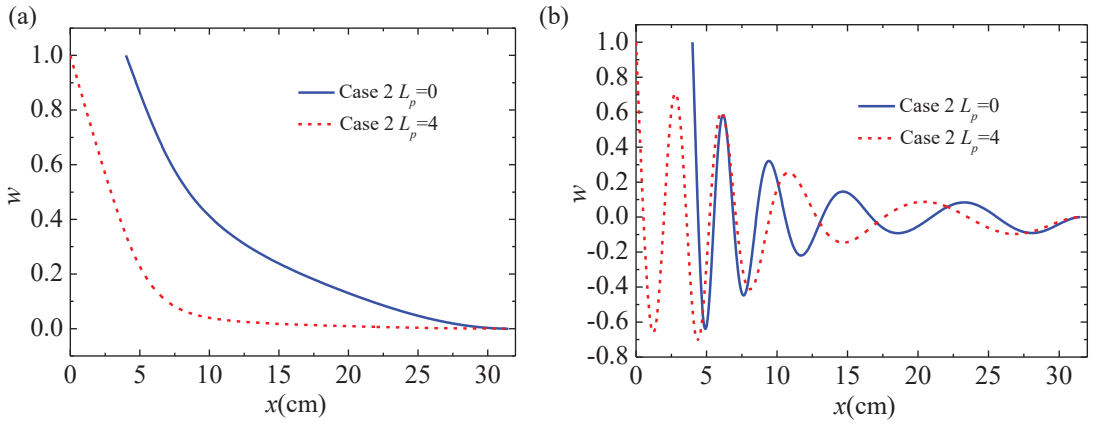

Fig. 10 Mode shapes with and without extended platform: (a) first mode, and (b) tenth mode.

Fig. 11 shows the system loss factors in case 2 with different extend platform lengths with damping layers. As the length increases, the system loss factor also increases in a broadband region, not necessarily proportional to the increase in the length of the platform. At lower frequencies, the damping enhancement is observable but not systematic for different lengths of the platform, depending on the modal behavior of the structure as mentioned before. Nevertheless, the observation that the first system modal loss factors increases and the effective frequency is shifted to lower frequencies with the increasing platform length still holds. Therefore, the length of the platform should be properly selected to target particular application frequency range with additional consideration of the system dimension.

4. CONCLUSIONS

An Euler-Bernoulli beam with a modified thickness profile and extended platform is investigated by using a previously developed wavelet-decomposed semi-analytical model. This model is shown to provide high accuracy through comparisons with experimental results. Given the same minimum achievable truncation thickness, a beam with a modified thickness profile is systemically investigated and compared with its counterpart having conventional ABH profile in terms of cross point mobility, energy distribution and the system loss factors. Numerical results show that the modified thickness profile can significantly improve the ABH effect at higher frequencies by promoting larger structural deformation at the ABH portion. This results in better energy concentrating on the ABH part, leading to the increased system damping and reduction of vibration amplitude when damping layers are applied.

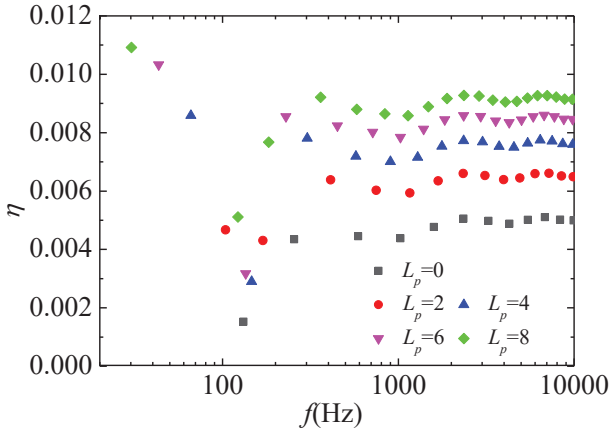

Fig. 11 Comparison of system loss factors for case 2 with different lengths of extended platforms when ABH part covered by damping layers (h_d = 0.02 cm).

The extended platform further enhances the overall system damping loss factor in the mid-high frequency range, and create a significant shift of the ABH effect towards lower frequency. The extended platform can significantly increase the first peak in the energy ratio curve and shift it to lower frequency, which provides the possibility of catering ABH effect for lower frequency applications.

In conclusion, for minimum truncation thickness which is the achievable by current manufacturing technology, an ABH wedge could be manufactured according the proposed modified thickness profile with an extended platform to enhance the ABH effect. The effect of other parameters defining the modified thickness profile, such as m, ε, will also be elaborated during the oral presentation.

ACKNOWLEDGEMENTS

This work is supported by the Research Grant Council of the Hong Kong SAR (PolyU 152009/15E and PolyU 152026/14E), National Natural Science Foundation of China (No. 11532006) and the NUAA State Key Laboratory Program under Grant MCMS-0516K02 for financial support.

REFERENCES

1. Krylov VV. Localised acoustic modes of a quadratically shaped solid wedge. Moscow University Physics Bulletin 1990; 45 (6): 65-69.
2. Krylov VV. Tilman FJBS. Acoustic 'black holes' for flexural waves as effective vibration dampers. Journal of Sound and Vibration 2004; 274 : 605-619.
3. Krylov VV. New type of vibration dampers utilizing the effect of acoustic black holes. Acta Acustica United with Acustica 2004; 90(5): 830-837.
4. O'Boy DJ, Krylov VV. Damping of flexural vibrations in circular plates with tapered central holes. Journal of Sound and Vibration 2011; 330: 2220-2236.
5. O'Boy DJ, Bowyer EP, Krylov VV. Point mobility of a cylindrical plate incorporating a tapered hole of power-law profile. Journal of the Acoustical Society of America 2011; 129(6): 3475-3482.
6. Georgiev VB, Cuenca J, Gautier F, Simon L, Krylov VV. Damping of structural vibrations in beams and elliptical plates using the acoustic black hole effect. Journal of Sound and Vibration 2011; 330: 2497-2508.
7. Bowyer EP, O'Boy DJ, Krylov VV. Damping of flexural vibrations in plates containing ensembles of tapered indentations of power-law profile. Proceeding of Meetings on Acoustics 2013; 18: 030003.
8. Krylov VV, Winward RETB. Experimental investigation of the acoustic black hole effect for flexural waves in tapered plates. Journal of Sound and Vibration 2007; 300: 43-49.
9. Bowyer EP, Krylov VV. Experimental study of Sound radiation by plates containing circular indentations of power-law profile. Applied Acoustics 2015; 88: 30-37.
10. Conlon SC, Fahnline JB. Numerical analysis of the vibroacoustic properties of plates with embedded grids of acoustic black holes. Journal of the Acoustical Society of America 2015; 137(1): 447-457.
11. Zhao LX, Conlon SC, Semperlotti F. Broadband energy harvesting using acoustic black hole structural tailoring. Smart Materials and Structures 2014; 23: 065021.
12. Zhao LX, Conlon SC, Semperlotti F. An experimental study of vibration based on energy harvesting in dynamically tailored structures with embedded acoustic black holes. Smart Materials and Structures 2015; 24: 065039.
13. Bowyer EP, O'Boy DJ, Krylov VV, Horner JL. Effect of geometrical and material imperfections on damping flexural vibrations in plates with attached wedges of power law profile. Applied Acoustics 2012; 73: 514-523.
14. Denis V, Pelat A, Gautier F. Scattering effects induced by imperfections on an acoustic black hole placed at a structural waveguide termination. Journal of Sound and Vibration 2016; 362: 56-71.
15. Bayod JJ. Experimental study of vibration damping in a modified elastic damping in a modified elastic wedge of power-law profile. Journal of Vibration and Acoustics 2011; 133: 061003.
16. Denis V, Gautier F, Pelat A, Poittevin J. Measurement and modelling of the reflection coefficient of an Acoustic Black Hole termination. Journal of Sound and Vibration 2015; 349: 67-79.
17. Tang LL, Cheng L, Ji HL, Qiu JH. Characterization of Acoustic Black Hole effect using a one-dimensional fully-coupled and wavelet-decomposed semi-analytical model. Journal of Sound and Vibration 2016; 374: 172-184.
18. Cheng L, Lapointe R. Vibration attenuation of panel structures by optically shaped viscoelastic coating with added weight considerations. Thin-Walled Structures 1995; 21: 307-326.
19. Cheng L. Vibroacoustic modeling of mechanically coupled structures: artificial spring technique applied to light and heavy medium. Shock and Vibration 1996; 3(3): 193-200.
20. Daubechies I. Ten lectures on wavelets. CBM-NSF conference series in applied mathematics, Philadelphia: SIAM ED, 1992.